Experimental analysis of total energy absorption capacity in RC beams subjected to drop weigh impact

Research Article

International Journal of
Protective Structures

Experimental analysis of total energy absorption capacity in RC beams subjected to single or repeated drop-weight impacts

International Journal of Protective Structures
2026, Vol. 17(2) 373–401

DOI: 10.1177/20414196251361155
journals.sagepub.com/home/prs

Morgan Johansson[1,2], Joosef Leppänen[1], Mathias Flansbjer[3], Fabio Lozano[1], Jack Jönsson[4], Josef Makdesi[5] and Anton Stenseke[6]

Abstract

Reinforced concrete (RC) protective structures require a large energy absorption capacity if they are to effectively withstand impulse loading due to blast or impact. Such structures may be subjected to both single and repeated impulse loading but there are just a few studies for the latter case. Therefore, in this study, experiments were conducted on RC beams, which were subjected to single or repeated drop-weight impacts. The beam response during impact was studied using a high-speed camera and digital image correlation. To determine the total energy absorption capacity, the impact-loaded beams were subjected to static loading until failure and the results compared to those of statically loaded reference beams. The total energy absorption capacity was of the same order or higher for beams previously subjected to impact loading, with a strong impact resulting in a greater increase. For tests in which the total impact energy was kept constant, repeated impact loading caused increased local damage, whilst decreasing the total energy absorption capacity.

Keywords

Reinforced concrete, experiments, energy absorption capacity, drop-weight impact, repeated impacts, digital image correlation

[1]Department of Architecture and Civil Engineering, Chalmers University of Technology, Göteborg, Sweden
[2]Norconsult Sverige AB, Göteborg, Sweden
[3]Division of Materials and Production, RISE Research Institutes of Sweden, Borås, Sweden
[4]Rochla Bygg AB, Vellinge, Sweden
[5]Sweco Sverige AB, Göteborg, Sweden
[6]Tyréns Sverige AB, Alingsås, Sweden

Corresponding author:
Joosef Leppänen, Department of Architecture and Civil Engineering, Chalmers University of Technology, Sven Hultins gata 6, Göteborg SE-412 96, Sweden.
Email: joosef.leppanen@chalmers.se

Introduction

Reinforced concrete (RC) protective structures, such as civil defence shelters or military fortifications, are designed to withstand the effects of extreme loading due to blast and impact. In such cases, the acting dynamic load typically consists of a high-pressure, short-duration load pulse, often referred to as an "impulse load". Impulse loads have very different properties compared to the static loads normally considered when designing a civil structure. Thus, an impulse-loaded structure may exhibit a structural response that differs in several respects from what is obtained with a corresponding static load. Furthermore, the high stiffness and load capacity properties normally desirable in a statically loaded structure are not necessarily required in an impulse-loaded one. Rather, it is the structure's energy absorption capacity that is important in effectively withstanding the effect of impulse loading. Protective structures are normally designed to withstand the effects of a defined threat, consisting of, say, a single explosive charge detonating at a certain distance. However, another reasonable scenario is that a structure may also be subjected to repeated impulse loading from several charges and, accordingly, such scenarios may also need to be considered in its design (Swedish Fortifications Agency, 2011).

Optimally, in this type of study, an impulse load would consist of an explosive blast wave. However, tests involving explosive charges are expensive and can be difficult to implement and evaluate. Therefore, the impulse load in this study was applied by using drop-weight impact. Although there are obvious differences between an impact and a blast load, the structural response obtained from either type still shows fundamental similarities. Single drop-weight impact tests are also commonly used to study the dynamic response of impulse-loaded RC beams (Adhikary et al., 2015; Fujikake et al., 2009; Johansson et al., 2024; Kishi et al., 2002; Saatci and Vecchio, 2009; Ulzurrun and Zanuy, 2024). However, studies of RC structures subjected to repeated impact loading are relatively scarce, indicating a lack of knowledge in this field. Such tests have been conducted on RC slabs by scholars including Batarlar et al. (2021), Othman and Marzouk (2016), Said and Mabrook Mouwainea (2022), Sharma and Kasilingam (2024), focusing on studying the response upon repeated impact loading and up until final failure, while Kang et al. (2025) conducted repeated impact loading tests comprising two consecutive impacts on post-tensioned RC beams. Thus, further investigation is warranted of the effect of repeated impact loading on the energy absorption capacity of RC structures, with particular emphasis on a structure's energy absorption capacity.

Typically, impact force, support reaction force, midspan deflections and final crack patterns are measured in drop-weight impact tests. Furthermore, to register the dynamic structural response, high-speed filming combined with digital image correlation (DIC) may be used to study responses such as strain fields, deflections or crack patterns (Reu and Miller, 2008). This has been used in some studies of RC beams, such as (Isaac et al., 2017; Johansson et al., 2024; Leppänen et al., 2020; Ulzurrun and Zanuy, 2024).

By performing static tests until failure on beams previously subjected to impulse loading, the residual (and, hence, also the total) energy absorption capacity of the beams may be estimated. Such tests have been performed by such scholars as Adhikary et al. (2015), Fujikake et al. (2006), Magnusson and Hallgren (2003), and Yilmaz et al. (2023). A common feature of these studies is that the residual load-deflection response corresponds rather well to that obtained in reference beams subjected solely to static loading. However, the focus on the total energy absorption capacity in these tests was limited. Only one test of each configuration was carried out, so the repeatability of the results was not investigated. Furthermore, the effect of repeated impulse loading was not investigated at all.

For the present study, two experimental series were conducted on RC beams subjected to single or repeated drop-weight impacts, followed by static loading with three or four-point bending. DIC was used to analyse the structural response of both statically loaded and impact-loaded beams. The aim was to investigate how the total energy absorption capacity of an RC beam is affected when it has been previously subjected to single or repeated impact loading. The novelty of this study lies in its focus on the beam's total

energy absorption capacity, determined through a combination of impact and static loading. Additionally, the study investigates the effects of multiple impacts, which is important for better understanding the response of protective structures subjected to repeated impulse loading.

Theoretical background

Dynamic structural response at impulse loading

It is well known that the structural response of impulse-loaded RC structures differs from statically loaded ones and that, consequently, the failure causes may differ. This is due partly to high strain rate effects, which increase the material stiffness and strength (Bischoff and Perry, 1991; Malvar, 1998; Malvar and Ross, 1998), and partly to inertia and wave propagation effects (Cui et al., 2023; Magnusson et al., 2014; Yi et al., 2016).

For impulse loading, the wave propagation effects are important. When a structure is subjected to a load, information travels within that structure at the speed of sound, which means some time elapses. The initial response is denoted as the local response (Fujikake et al., 2006). The deformed shape of a beam subjected to an impact will vary, as illustrated schematically in Figure 1. In this figure, a plastic hinge is assumed to form at the impact point with only some parts of the beam initially affected by the impact. The structural response will then resemble that of a fixed beam but with a time-dependent boundary condition (BC), in which the effective span length l_{eff} gradually increases with a propagation velocity v_F. This velocity varies with time and decreases approximately in proportion to increased beam slenderness (Ulzurrun et al., 2019). When the effective length reaches the supports, if the beam is not vertically restrained, it will elevate briefly (Lovén and Svavarsdóttir, 2016). Once the entire beam is affected, the overall response is initiated and a deformed shape, approximately corresponding to that of static loading, is obtained (Fujikake et al., 2009).

The ability of a structure to withstand the effect of impulse loading depends on the external energy applied to it and its energy absorption capacity. Ideally, the absorption capacity is determined by major deformations rather than large, internal structural forces (Biggs, 1964; DOD, 2008; Swedish Fortifications Agency, 2011). This is ensured by designing the structure in terms of bending and providing it with enough plastic deformability to produce a major deflection prior to failure. To fulfil this criterion, the structure must be designed so that there is no premature brittle failure due to, say, shear. Hence, it is essential to avoid shear failure in an impulse-loaded structure. However, a potential problem is that the mechanics of shear failure in such structures are not as well-understood as bending failure (Kishi et al., 2002). Thus, shear failure in impulse-loaded structures has been the focus of several studies. These have observed that a statically loaded

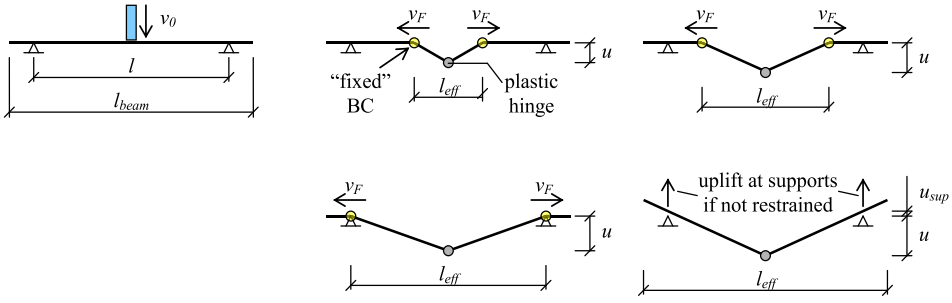

Figure 1. Schematic illustration of how the deformed shape of an impact-loaded beam develops during the initial local response when not vertically restrained at the supports. From (Leppänen et al., 2020); based on (Lovén and Svavarsdóttir, 2016; Yi et al., 2016).

structure that fails due to bending may, instead, fail in shear when subjected to impulse loading (Kishi et al., 2002; Magnusson et al., 2014; Saatci and Vecchio, 2009).

For impact loading, the external energy acting on a structure depends mainly on the impact mass and velocity and the effective mass of the relevant structure. The geometry of the impactor may also be important (Li et al., 2020; Mier et al., 1991; Zhang et al., 2023). Having an impactor nose head of decreased radius (a sharper nose) increases that nose head's local pressure and thus also the penetration of the impactor into the structure. This may lead to severe local damage at the impact zone but will also result in reduced contact stiffness and thus decreased impact force. Hence, an increased nose head radius (a flatter nose) results in increased contact stiffness between impactor and structure and thus also increased impact force. However, since the impact impulse remains the same, an increased impact force results in a shorter initial load pulse from the impact. Consequently, the nose head radius may affect the risk of local (spalling or shear) failure in the impacted structure. However, if this is not the case the global structural response will not be influenced much by the geometry of the impactor (Pham et al., 2018).

When unloading, the elastic energy $W_{i,el}$ gathered in the structure will cause the structure to rebound. If unrestrained, this will cause the structure to lose contact with its supports, see Figure 1. This means that restrained boundary conditions may significantly affect the response of the rebounded beam, although they will probably have a negligible effect on the critical response (up to maximum deflection in the direction of the applied load). This was the case in Leppänen et al. (2020) who also showed that before rebounding occurs, the midpoint deflection and crack propagations are very similar for restrained or unrestrained support boundary conditions.

Energy balance of external and internal work

The kinetic energy $E_{k,0}$ and kinetic impulse I_0 of the impactor just prior to impact with a structure may be determined as:

$$E_{k,0} = \frac{m_w \cdot {v_0}^2}{2} \tag{1}$$

$$I_0 = m_w \cdot v_0 \tag{2}$$

in which m_w is the mass of the impactor and v_0 is its velocity at impact. Assuming a plastic impact, the velocities of the impactor and impacted structure remain the same after impact. With the conservation of momentum before and after impact, the velocity v_{wb} after impact may be derived as:

$$v_{wb} = \frac{m_w}{m_w + m_b} \cdot v_0 \tag{3}$$

in which m_b is the effective mass of the structure. Using equation (1), the external work $W_{e,k}$, caused by the kinetic energy and acting on the structure due to impact, may be formulated as:

$$W_{e,k} = \frac{(m_w + m_b) \cdot {v_{wb}}^2}{2} = \frac{m_w}{m_w + m_b} \cdot \frac{m_w \cdot {v_0}^2}{2} = \frac{m_w}{m_w + m_b} \cdot E_{k,0} \tag{4}$$

This means that an impact with impact energy $E_{k,0}$ will produce greater external work $W_{e,k}$ on the structure when the impact mass m_w is high and the effective mass m_b is low.

Prior to the release of the impactor, its potential energy may be expressed as:

$$E_{p,0} = m_w \cdot g \cdot h_w \tag{5}$$

in which $g = 9.81$ m/s^2 is the gravitational acceleration and h_w is the drop height of the impactor, Since energy is only transformed and never lost, the kinetic and potential energy remain the same; that is $E_{k,0} = E_{p,0}$. Thus, setting the expressions in equations (1) and (5) as equal, the impact velocity v_0 may be derived as:

$$v_0 = \sqrt{2 \cdot g \cdot h_w} \tag{6}$$

Consequently, even though the impact energy $E_{k,0}$ is constant, an impactor with mass $m_w = 2 \cdot m$ and drop height $h_w = h$ will produce greater external work $W_{e,k}$ on the structure than an impact caused by an impactor with mass $m_w = m$ and drop height $h_w = 2 \cdot h$.

If the impact acts in the same direction as gravitational acceleration, the deflections in the impact-loaded structure will cause an additional loss of potential energy for both the impactor and the structure. This loss of energy is converted into additional external work $W_{e,p}$ acting on the structure. If the impact occurs at the midpoint of a beam, causing a plastic response (triangular-shaped deflection) with a maximum beam midpoint deflection u_{max}, this may be determined as:

$$W_{e,p} = \left(m_w + \frac{m_{beam}}{2}\right) \cdot g \cdot u_{\max} \tag{7}$$

in which m_{beam} is the mass of the beam. The total external work can then be determined as:

$$W_{e,tot} = W_{e,k} + W_{e,p} \tag{8}$$

The structural response of an impulse-loaded structure is based on energy balance. The external work $W_{e,tot}$ applied by the external load $F(u)$ is balanced by the internal work (that is, the energy absorption capacity):

$$W_i = \int R(u)du \tag{9}$$

in which $R(u)$ is the load capacity as a function of the deflection u. If the internal work is high enough ($W_i \geq W_{e,tot}$), the structure withstands the effect of impulse loading and will reach its maximum deflection when $W_i = W_{e,tot}$.

Figure 2 illustrates a simplified case in which an impulse load (giving rise to the external work $W_{e,1}$) has been applied to a structure with bilinear load capacity $R(u)$. $W_{e,1}$ is balanced by the structure's internal work $W_{i,1}$, resulting in a total deflection u_1. This deflection consists of an elastic ($u_{el,1}$) and a plastic ($u_{pl,1}$) component, contributing to the internal work $W_{i,el,1}$ and $W_{i,pl,1}$ respectively. Once u_1 is reached, elastic unloading occurs (but no rebound is included in the figure), resulting in a final plastic deflection $u_{0,1} = u_{pl,1}$ (a permanent deflection at zero load). Accordingly, if the same structure is loaded again, this time with an impulse causing the external work $W_{e,2}$, the deflection will start at $u_{0,1}$. The second loading causes an additional deflection $u_2 = u_{el,2} + u_{pl,2}$, ending up with a total deflection $u_{tot,2} = u_{pl,1} + u_2$. Theoretically, since the structure's elastic stiffness and load capacity R_{Rd} are assumed to remain the same, the elastic internal work $W_{i,el,2}$, caused by the external work $W_{e,2}$, will be the same as $W_{i,el,1}$. Hence, based on this reasoning, the total internal work $W_{i,tot}$ needed in a structure to withstand the effect of n number of impulse loads (each giving rise to an external work $W_{e,j}$) may be expressed as:

$$W_{i,tot} = W_{i,el} + W_{i,pl,tot} \tag{10}$$

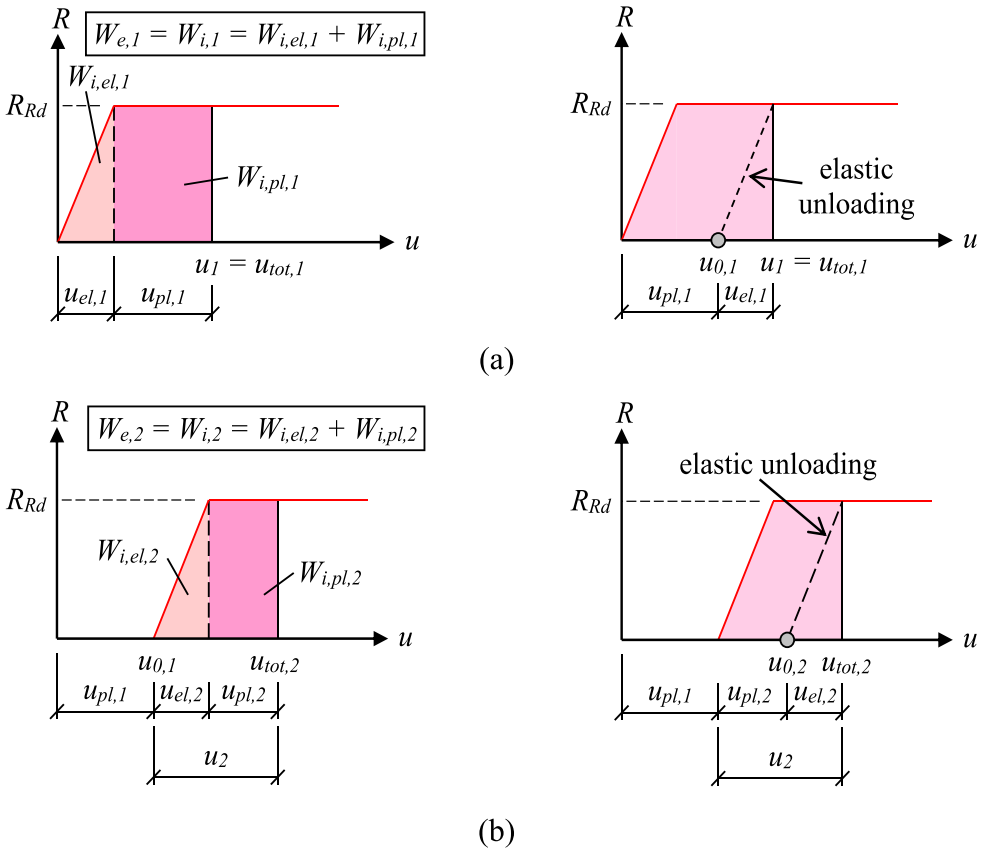

Figure 2. Schematic illustration of structural response when subjected to impulse-loading, due to (a) single impact and (b) repeated impact. Based on (Johansson and Laine, 2012).

in which

$$W_{i,pl,tot} = \sum_{j=1}^{n} W_{e,j} - n \cdot W_{i,el} \tag{11}$$

The real $R(u)$ curve of the structure is more complex than indicated in Figure 2. Also, if damage is sustained under loading, both the elastic stiffness and load capacity R_{Rd} may be further reduced, thus affecting both the elastic and plastic values of the internal work $W_{i,tot}$.

Experimental test set-up

Geometry and material properties

The experiments reported here were conducted as two test series, designated Series I (Lozano and Makdesi, 2017) and Series II (Jönsson and Stenseke, 2018). The experimental results and processed data are available in Leppänen (2025). In both series, drop-weight impact tests were conducted on

RC beams. Static tests were then carried out on these beams, using three or four-point bending, up until final failure. Both series also tested reference beams that were subjected only to static loading.

The beams in both series had identical geometry and reinforcement amount. The length of the beams was 1180 mm, with a span length of 1000 mm and a beam cross-section of 100 × 100 mm. These beams were reinforced with 2 + 2 ribbed 6 mm steel bars, with a nominal effective depth of 80 mm. The beams were cast using two different concrete mixtures of self-compacting (Series I) or conventional concrete (Series II), see Table 1 for the recipes. The compressive cube strength $f_{c,cube}$ and fracture energy G_F were tested according to CEN (2009), Löfgren et al. (2004) and the resulting material parameters appear in Table 2. The compressive strength was tested on cubes and the cylinder compressive strength was then determined as $f_c = 0.8 \cdot f_{c,cube}$. Compressive tests were carried out on both day-of-impact testing (Series I: 36 days; Series II: 26 days) and at a concrete age of 28 days ($f_{c,28d}$).

Material tests on the reinforcement were conducted for both series. Class C reinforcement with a characteristic yield strength f_{yk} = 500 MPa (CEN, 2004), supplied in coils, was used. Coil reinforcement is transported in rolls and then straightened before use, resulting in mechanical properties somewhat similar to cold-worked reinforcement. Thus, the proof stress $f_{0.2}$ was used to describe the reinforcement, alongside the tensile strength f_t and reinforcement strain ε_u at tensile strength f_t.

This study used small-scale experiments with geometries similar to those in studies such as Barr and Bouamrata (1988) and Zhang et al. (2010). However, in concrete structures, there is a size effect that will influence the rotational capacity of a structure (Bigaj, 1999; Carpinteri et al., 2009), making the response more brittle with increased depth. This means that the use of small-scale specimens will present larger plastic deflections and thus also greater energy absorption capacity than would be the case in RC structures of greater depth. Nevertheless, the effect on the conceptual structural response and energy absorption capacity is still noteworthy. Moreover, the results are also suitable for use in verifying other results obtained using nonlinear, finite element analyses.

Drop-weight impact tests

In the experiments, a steel drop-weight of varying mass was released to impact simply supported RC beams, as illustrated in Figure 3. The test set-up was made as simple as possible and comprised a simply supported beam. The supports comprised steel cylindrical supports (Series I) or fixed half-cylindrical supports (Series II) with a diameter of 70 mm. The boundary conditions in Series II were changed to further

Table 1. Concrete recipe in series I and II.

	Amount (kg/m^3)	
Material	Series I	Series II
Cement	335	330
Limestone filler	160	—
Sand	747.3	947.4
Aggregate, 4–8 mm	268.9	96.6
Aggregate, 8–16 mm	717.1	819.4
Superplasticiser	5.36	5.36
Water	184.3	194.7
w/c ratio	0.55	0.59

Table 2. Material properties of concrete and steel reinforcement; mean values and standard deviations (given within parentheses) are based on three to six tests for concrete and seven tests for reinforcement.

	Concrete			Steel reinforcement			
	f_c	$f_{c,28d}$	G_F	$f_{0.2}$	f_t	f_t / $f_{0.2}$	ε_u
Series	(MPa)	(MPa)	(N/m)	(MPa)	(MPa)	[-]	(‰)
I	42.2 (2.8)	40.0 (1.8)	132 (18)	575 (9)	686 (4)	1.19 (0.02)	108 (9)
II	29.5 (0.7)	29.4 (1.8)	137 (1)	513 (11)	623 (10)	1.21 (0.01)	106 (5)

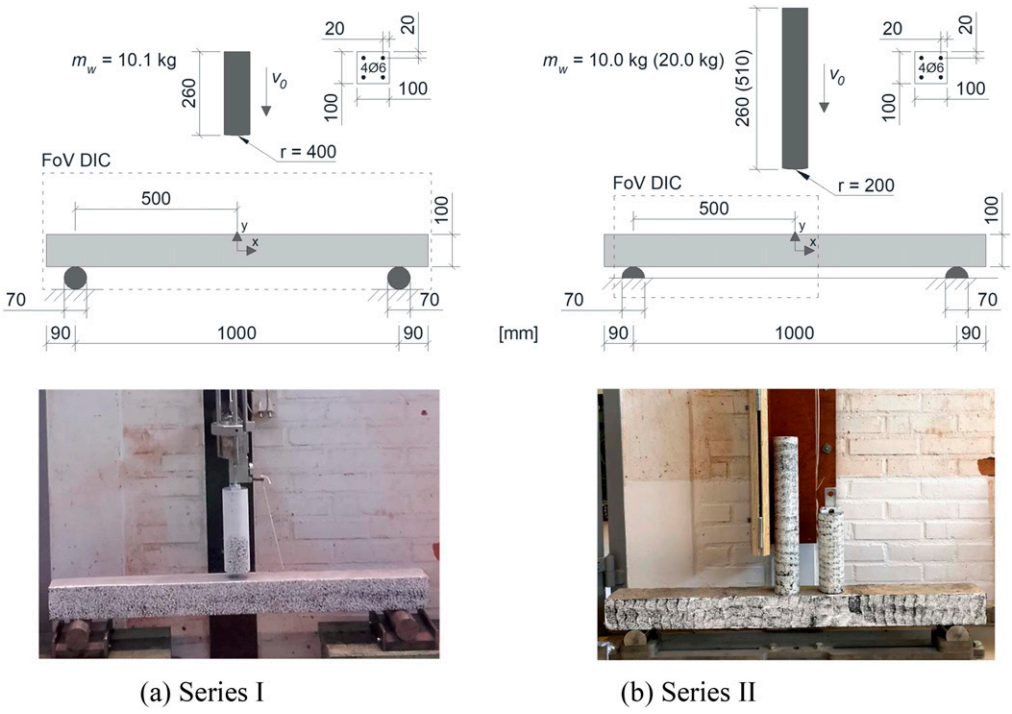

(a) Series I (b) Series II

Figure 3. Drop-weight impact tests, geometry and test set-up for (a) Series I, with guiding steel rails visible at the top of the photo, and (b) Series II, wherein both drop-weights are shown in the photo. The field of view (FoV) of the high-speed camera is marked in each series.

simplify the test set-up; this was not deemed to influence the results. To avoid any support moments, no vertical restraint on top of the beam was used. High-speed filming was used to record dynamic response but the impact load and support reactions were not measured. A summary of the two test set-ups is shown in Figure 3.

A real beam is typically vertically restrained at its supports, and in many impact tests, this has been added to prevent uplift due to initial response and rebounding (Fujikake et al., 2009; Kishi et al., 2002; Saatci and Vecchio, 2009). However, it is also common to use a test set-up with no upper vertical restraint (Adhikary et al., 2012; Barr and Bouamrata, 1988; Zhang et al., 2010). If no upper vertical restraint is used,

Table 3. Classification of tested beams with nominal input.

Series	Beam	m_w (kg)	h_w (m)	n [no.]	v_0 (m/s)	$E_{k,0}$ (J)	I_0 (N·s)	$n \cdot E_{k,0}$ (J)	$n \cdot I_0$ (N·s)
I-1	IB-01, IB-02, IB-03, IB-10, IB-11, IB-12	10.1	2.5	1	7.0	248	71	248	71
I-2	IB-04, IB-05, IB-06, IB-13, IB-14, IB-15	10.1	5.0	1	9.9	495	100	495	100
I-Ref	IB-07, IB-08, IB-09, IB-16, IB-17, IB-18	—	—	—	—	—	—	—	—
II-1	IIB-04, IIB-05, IIB-06	10.0	2.5	4	7.0	245	70	981	280
II-2	IIB-01, IIB-02, IIB-03	10.0	5.0	2	9.9	491	99	981	198
II-3	IIB-13, IIB-14, IIB-15	20.0	2.5	2	7.0	491	140	981	280
II-4	IIB-10, IIB-11, IIB-12	20.0	5.0	1	9.9	981	198	981	198
II-Ref	IIB-07, IIB-08, IIB-09, IIB-16, IIB-17, IIB-18	—	—	—	—	—	—	—	—

it is suitable to focus on the initial structural response up to the maximum beam deflection. The beams in the test series reported here had no vertical restraint, primarily to provide boundary conditions that were as well-defined as possible and avoid the risk of adding any restraint moments at the supports. Since the focus of the dynamic tests was to study the beam's structural response up to maximum deflection, the influence of not using a vertical restraint was deemed negligible.

Three different drop-weight masses and two drop heights were used in the tests, see Table 3. Each load configuration was tested on three or six specimens, thus allowing the potential repeatability of the observations to be investigated. The drop-weight consisted of a solid steel cylinder with a spherical impact surface of radius r and was guided using three vertical steel rails which formed a pipe. No protective layer was placed between the impactor and the beam, meaning that the impact was applied directly to the concrete. Drop heights h_w of 2.5 m and 5.0 m were used, resulting in (see equation (6)) impact velocities v_0 of approximately 7.0 m/s and 9.9 m/s respectively. The drop-weight had a mass of 10.1 kg in Series I and 10.0 or 20.0 kg in Series II, see Figure 3 for more information on its geometry.

Static tests

Once subjected to drop-weight impact tests, the beams were statically loaded until failure, whereupon load-deflection curves were registered using a load cell and displacement transducer. Reference beams were tested in static loading only and used for comparison with the impact-loaded beams.

The beams were simply supported and placed on the same type of steel cylinders used in the impact tests in Series I. The load was applied using displacement-controlled loading and tested under three-point (Series I) or four-point bending (Series II), as shown in Figure 4.

In Series II, there was substantial damage to the impact zone in those beams subjected to repeated impact. These beams could not, therefore, be tested in three-point bending, so static loading was applied instead using four-point bending. In both test series, the beams were supported on steel rollers placed on thick, solid steel plates. A displacement rate of 2 mm/min was used for the initial displacement (Series I: $u = 0$–10 mm, Series II: $u_F = 0$–40 mm). A rate of 10 mm/min was then used in both test series. Additionally, to study the resulting change in stiffness in different stages, the reference beams in Series II were unloaded and reloaded at displacements of 10 mm, 20 mm and 40 mm, at a rate of 2 mm/min.

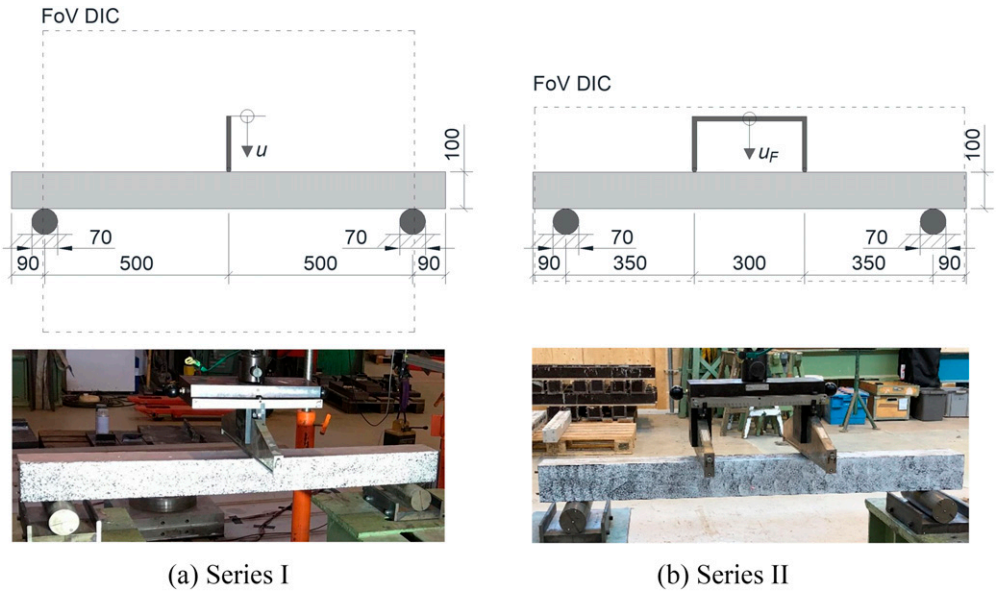

Figure 4. Static test set-up, (a) Series I and (b) Series II. The field of view (FoV) of the stereoscopic camera is marked in each series.

The estimated load capacities in Series I were about 11 kN due to bending and about 19 kN due to shear force. In Series II the load capacities were 13 kN and 17 kN, respectively. Thus, failure due to bending moment was anticipated in both test series.

Photographic imaging and DIC

In both the dynamic and static tests, the structural response of the beams was analysed using digital image correlation (DIC). This measurement technique is typically used to measure displacement fields and surface strain fields in planar, two-dimensional situations using a single camera (2D-DIC) set-up and in three-dimensional situations using a stereoscopic camera (3D-DIC) set-up. Images from high-speed filming were used for DIC analyses, to register deflections and crack propagation in beams subjected to impact loading. For the static loading, the load and midpoint deflection were measured and DIC was used to evaluate the crack propagation.

The DIC concept involves measuring the deformation of a specimen during testing. This is done by analysing the deformation of a surface speckle pattern in a series of digital images acquired during loading. This is accomplished by tracking discrete pixel subsets of the speckle pattern within the images. To determine the displacement of any subset, it is necessary to match a region of the reference image with a deformed image and match the left and right cameras in a 3D set-up. The unique, grey-value speckle pattern of each subset is used to perform correlation calculations so that the mid-point coordinates of the subsets may be tracked with sub-pixel accuracy. A correlation process is used to find the best match for each subset in the deformed image, relative to a reference image. Within the iterative correlation algorithm, the squares of the grey value differences are minimised for each subset. In this study, a bicubic subpixel interpolation together with a pseudo-affine shape function was used for the subset correlation. In GOM Correlate (GOM, 2018), the specimen surface is represented by triangles connecting measuring points,

defined by the mid-points of the subsets. The deformations of the specimens are calculated by correlating the positions and displacements of subsets in the undeformed reference image and deformed images to produce a deformation vector field. The surface strain tensor at each measuring point is then computed based on deformations at adjacent points, as represented by an equilateral hexagon. In this study, technical strains were calculated using a strain tensor neighbourhood size equal to one; in other words, the six closest adjacent points. No temporal or spatial filtering was used in post-processing the results. A comprehensive description of the measurement technique may be found in such works as Sutton et al. (2009) and Reu (2012).

DIC measurements have proved suitable for studying concrete structures when there is interest in studying cracking in detail. The propagation of individual cracks may be monitored at the surface long before they are visible to the naked eye, with a high degree of accuracy in local width development tracking.

The subset size influences both the resolution of the measured quantity and the spatial resolution. Typically, a larger subset improves the resolution at the expense of decreased spatial resolution and vice versa. The spatial resolution of the results is defined as the distance between independent measurement points (Pritchard et al., 2013). To capture result gradients (such as strain localisations caused by cracking), the data-point spacing is usually reduced by overlapping the subsets. However, since these subsets now share information with neighbouring subsets, the data points are no longer truly independent. At a given amount of subset overlap, no new information is added to the measurement data, even though the data-point spacing is reduced. Therefore, the subset step size defines the distance between the adjacent data points, while the subset size defines the spatial resolution of independent displacement data. Hence, the choice of subset size and subset overlap is often a question of finding a good compromise between spatial resolution and result resolution. The resolution of a measured quantity may be defined as the smallest value that may be detected above noise. One way to quantify this is to obtain at least two static images of the test object with no loading and then calculate the standard deviation for the quantity of interest (Pritchard et al., 2013). This is not the actual resolution but will indicate the lowest reliable value in the current configuration. A detailed study of the influence of subset size and subset overlap on the results for some of the impact-loaded beams tested in Series II was conducted by Johansson et al. (2019).

The drop-weight impact tests were investigated using high-speed 2D-DIC measurements. The images were acquired with a Photron FASTCAM SA4 high-speed camera at a rate of 5000 frames per second (fps), corresponding to a time resolution of 0.2 ms. For the tests, the camera was fitted with a Tamron 28–75/2.8 lens, with its focal length set to 28 or 75 mm and an aperture of f/4. Different fields of view (FoV) were applied in the test series, see Figure 3.

In Series I, the entire beam was covered to capture any asymmetric response. However, the resolution turned out to be unsatisfactory and therefore, the FoV in Series II, was reduced to cover slightly more than half the beam and increase the image resolution. The camera was positioned perpendicular to the main beam axis, at a distance that gave the desired field of view on the specimen. Information on the camera configurations used in the test series appears in Table 4, along with the spatial resolution, data-point spacing and displacement resolution used in DIC.

The speckle pattern used for the subset correlations was achieved by first applying white retro-reflective paint as a background and then black stains using a natural sponge. The specimen was illuminated by a high-power white LED light panel during testing, so as to obtain high contrast levels. The start of the high-speed imaging was triggered upon the drop-weight impact with a centre-mode recording, meaning that an approximately equal number of images were recorded before and after the impact. The images from the high-speed camera were analysed by a DIC technique using the GOM Correlate Professional (GOM, 2018). The choice of subset size was based on a parameter study of how subset size influences displacement resolution. This may be related to the standard deviation of the displacement components as

Table 4. Configuration of high-speed 2D-DIC and static 3D-DIC measurements.

		Impact tests		Static tests	
Parameter	Unit	Series I	Series II	Series I	Series II
Measuring distance	(mm)	1780	2225	1150	1330
Focal length	(mm)	28	75	24	24
Image size	(Pixels × pixels)	1024 × 304	1024 × 512	4096 × 3072	4096 × 1536
Field of view (FoV)	(mm × mm)	1200 × 360	630 × 315	1010 × 820	1170 × 475
Spatial resolution (subset size)	(Pixels)	21	15	24	24
	(mm)	24.6	9.2	5.9	6.9
Data point spacing (subset step)	(Pixels)	5	5	20	20
	(mm)	5.9	3.1	4.9	5.7
x-displ. resolution	(μm)	7.7	7.0	3	3
y-displ. resolution	(μm)	7.4	7.1	3	3
z-displ. resolution	(μm)	—	—	6	6

described earlier, see Figure 5. To achieve a combination of low noise and a data-point spacing that gives a clear crack visualisation, the dimensions of each subset were set to 21 × 21 pixels in Series I and 15 × 15 pixels in Series II, while the subset step in both cases was five pixels.

In the static tests, 3D-DIC measurements with a stereoscopic camera set-up were performed using the ARAMIS 12M system (Aramis, 2018). The cameras were fitted with Titanar lenses with a focal length of 24 mm. The system configuration was calibrated for an FoV covering slightly more than the distance between the supports in Series I and the entire length of the beam in Series II. The images were captured at frequencies of 1/2 and 1/3 fps for Series I and Series II respectively. The dimensions of each subset in the static tests were 24 × 24 pixels and the subset step was 20 pixels.

Results of drop-weight impact tests

Effect of wave propagation

Figure 6 shows the relative deflection $u(x)/u_{mid}$ of beam IIB-04 for the first 2 ms after impact, with $u(x)$ as the deflection in coordinate x and u_{mid} as the deflection in the middle of the beam, in the same time step. The results confirm the behaviour that was described schematically in Figure 1; that it takes some time for the impact load to transfer to the supports and thus for the beam's final deformed shape to develop. Directly after impact, the beam exhibits significant positive curvature beneath the impact zone, leading to the formation of a plastic hinge when the bottom reinforcement in this region yields. The deformation of the beam (represented here by a zone of negative curvature and tensile stresses in the top of the beam) then travels rapidly through the beam towards the supports. The tensile stresses may initiate cracking at the top of the beam, thus explaining the crack pattern observed 0.6 ms after impact. Eventually, the zone of negative curvature reaches the support and the beam lifts slightly from the support. Hence, the beam experiences something that may be described as time-dependent boundaries. Then, after about 2 ms, the beam reaches a deformed V-shape that corresponds to a beam loaded with a static load, in which a plastic hinge has developed at the middle of the beam. At this stage of loading, the cracks at the top of the beams are closed again and flexural shear cracks have started to develop. These shear cracks are also more pronounced at greater drop heights.

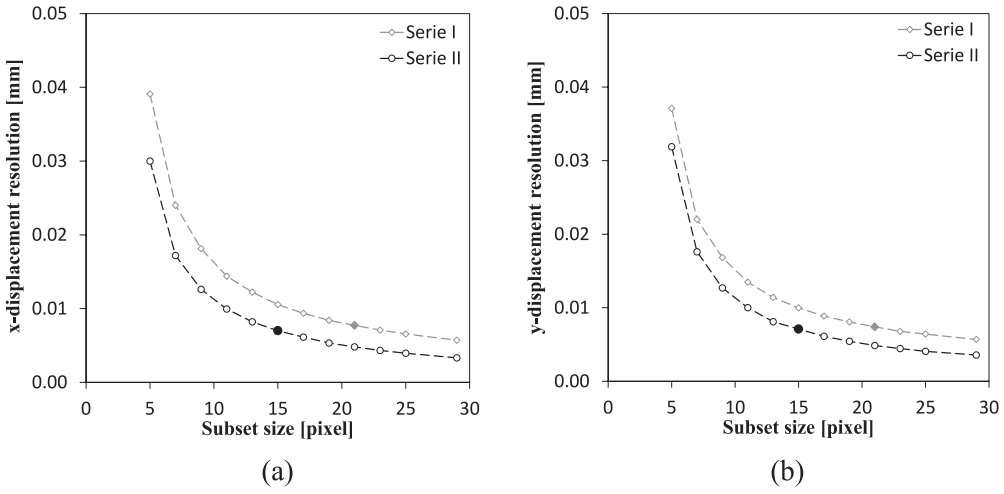

Figure 5. Influence of subset size on the displacement resolution, presented as the standard deviation of (a) x-displacement and (b) y-displacement component. Selected subset sizes are marked with solid markers.

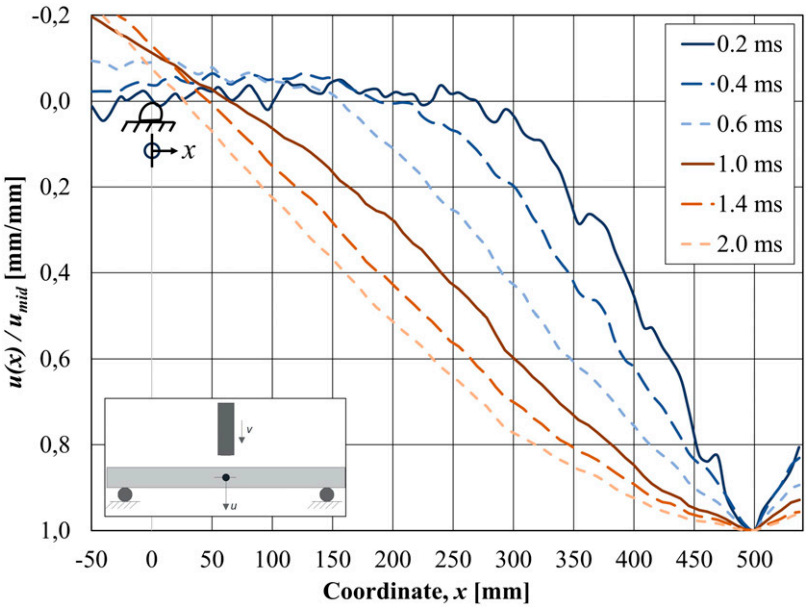

Figure 6. Relative deflection $u(x)/u_{mid}$ in beam IIB-4 (m_w = 10.0 kg, h_w = 2.5 m), during the initial 2 ms after impact.

Midpoint deflection

Figure 7 shows the modified midpoint deflection over time, $u_{mod}(t)$, from all single impact tests, plus the first impact for those beams subjected to repeated impacts. The scatter in the midpoint deflection for all tested beams was small, which shows that the repeatability of the tests was high. The results in Figure 7(a) and (b)

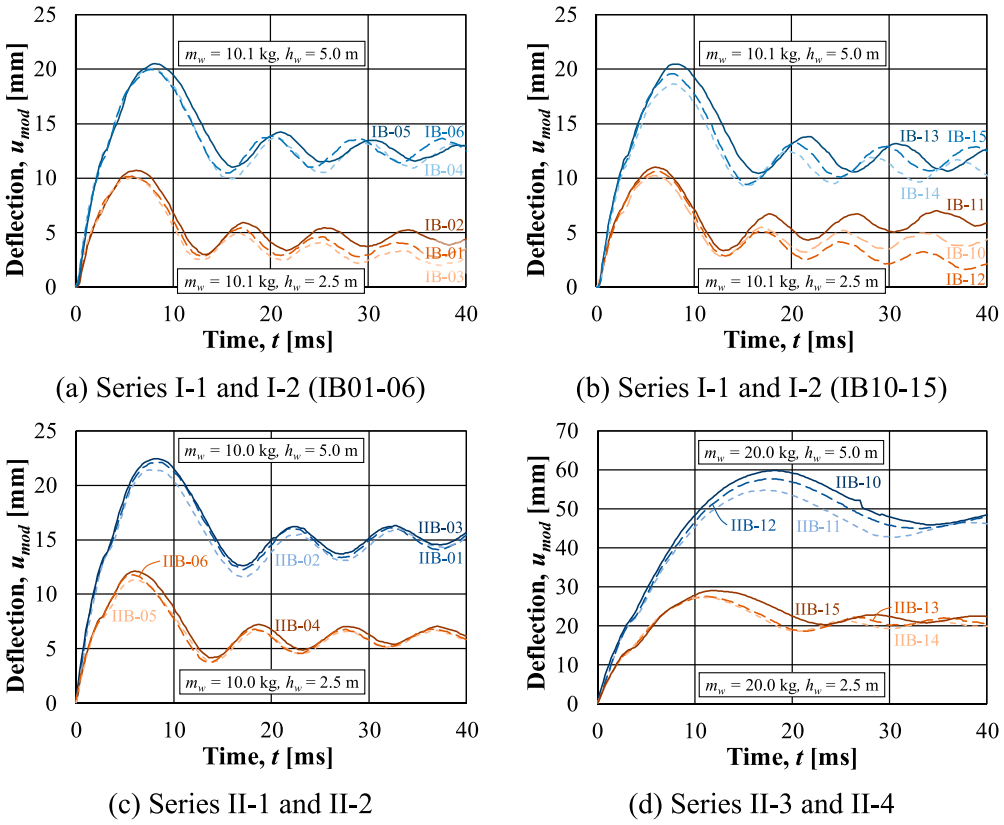

Figure 7. Modified midpoint deflection $u_{mod}(t)$ of first impact, where $u_{mod} = u - u_{sup}$ when using parameters defined in Figure 1.

(Series I) and c (Series II) may be directly compared. The load conditions were almost identical but the maximum deflections in Series I were somewhat smaller, due to the greater concrete and reinforcement strength (see Table 2).

Table 5 shows the accumulated midpoint deflections for repeated impacts in Series II. The accumulated maximum midpoint deflection $u_{tot,j}$ and accumulated plastic deflection (that is, permanent deflection at zero load) $u_{0,j}$ is shown for each impact j. The beams in Series II-1 were subjected to four impacts while those in Series II-2 and II-3 were subjected to two impacts each. The damage (denoted here as cracking, spalling and crushed concrete) increased with each impact, resulting in a reduction of the beams' effective depth and stiffness. Therefore, the additional maximum midpoint deflection obtained upon each impact also increased. It may also be observed that, as the impact energy and number of impacts increased, so did the scatter in maximum midpoint and plastic deflection.

Figure 8 shows the deflection-time curves for repeated impact for beam IIB-06 upon each impact (maximum midpoint deflection is $u_j = u_{tot,j} - u_{0,j-1}$, see Figure 2 for denotations and Table 5 for values). It may be observed that the maximum midpoint deflection u_2 for the second impact was only slightly greater than deflection u_1 for the first one. However, for the third and fourth impacts, the midpoint deflections u_3 and u_4 increased noticeably due to the accumulated damage from previous impacts.

Table 5. Maximum accumulated midpoint deflections for repeated impacts, see Figure 2 for denotations used. Mean values (standard deviations) are shown in bold.

Identification		Impact 1		Impact 2		Impact 3		Impact 4	
Series	Beam	$u_{tot,1}$ (mm)	$u_{0,1}$ (mm)	$u_{tot,2}$ (mm)	$u_{0,2}$ (mm)	$u_{tot,3}$ (mm)	$u_{0,3}$ (mm)	$u_{tot,4}$ (mm)	$u_{0,4}$ (mm)
II-1	IIB-04	12.1	5.9	19.1	12.0	27.7	18.6	48.9	39.0
	IIB-05	11.4	5.1	18.0	11.2	25.6	18.7	35.4	22.3
	IIB-06	11.8	5.1	17.1	10.1	24.2	16.0	31.6	19.4
	mean (std dev)	11.7 (0.4)	5.4 (0.5)	18.1 (1.0)	11.1 (1.0)	25.8 (1.8)	17.8 (1.5)	38.6 (9.1)	26.9 (0.39)
II-2	IIB-01	22.1	14.6	38.0	31.0				
	IIB-02	21.4	13.8	40.3	28.1				
	IIB-03	22.4	14.3	40.5	31.2				
	mean (std dev)	22.0 (0.5)	14.2 (0.4)	39.6 (1.4)	30.1 (1.7)				
II-3	IIB-13	27.5	20.1	54.0	40.9				
	IIB-14	27.3	20.3	54.4	44.4				
	IIB-15	29.0	21.8	61.2	49.2				
	mean (std dev)	27.9 (0.9)	20.7 (0.9)	56.5 (4.0)	44.8 (4.2)				

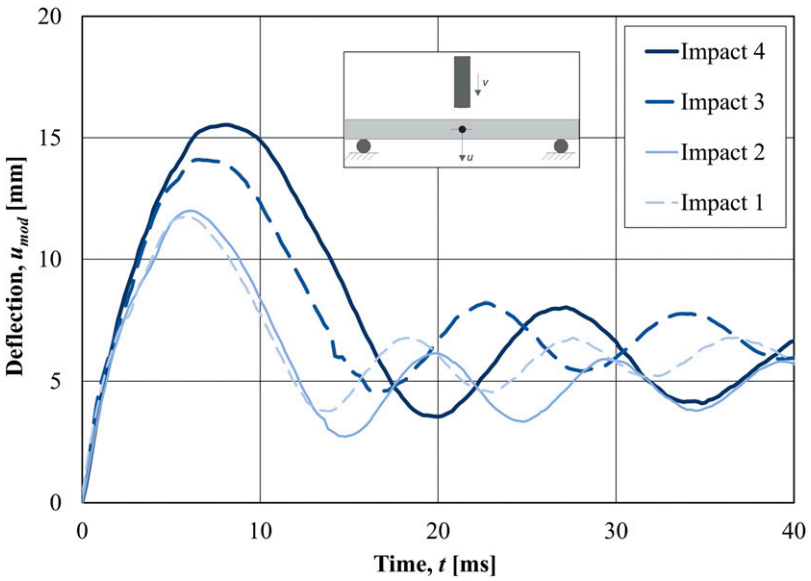

Figure 8. Deflection-time curves for repeated impacts in beam IIB-06 (m_w = 10.0 kg, h_w = 2.5 m).

Crack formation

High-speed photography was used in conjunction with a DIC technique to study the crack propagation during the impact tests. Figure 9 shows the crack propagation during the first 2 ms and at maximum midpoint deflection. These results are for one beam, representative of each type in Series II. Strain fields in the beams are shown in black and correspond to a 2% strain, a value selected to effectively visualize the cracks that formed, while individual black dots are due to noise in the results. In all tests, bending cracks formed immediately after impact at the bottom of the beam below the impact zone. After about 0.4 to 0.6 ms, bending cracks also formed at the top of the beam at roughly 0.25 m from the support. This was due to wave propagation effects. When subjected to higher impact loads in Series II-2 to II-4, diagonal shear cracks developed close to the impact zone. These shear cracks were more pronounced for the impacts caused by using an increased drop height (compare beams IIB-01 and IIB-12 with beams IIB-04 and IIB-13). Moreover, flexural shear cracks developed in all beams at approximately one-quarter of the span length from the support.

Figure 10 shows the crack formations for one beam of each type that were subjected to repeated drop-weight impacts (Series II). Most main cracks formed during the first impact and when subjected to repeated impacts, with the crack widths increasing upon each new impact. Furthermore, for repeated impacts, the crushing of the compressive zone at the top of the beam and spalling in the tensile zone at the bottom increased with each impact. Spalling on the beam's front face caused a loss of the surface pattern used for DIC analyses. These are shown as white areas in Figure 10.

All the beams in Series II were subjected to the same total impact energy $n{\cdot}E_{k,0}$, see Table 3. Nevertheless, the beam with the lowest mass and drop height, IIB-04 in Figure 10, resulted in the greatest damage. This indicates that repeated, lower-magnitude impacts cause more damage than a single larger impact containing the same total impact energy. A possible explanation for this is that in a beam subjected to repeated impacts, local damage occurs in the impact zone, causing increased crushing and spalling with each impact. Another observation is that the beam that was subjected to

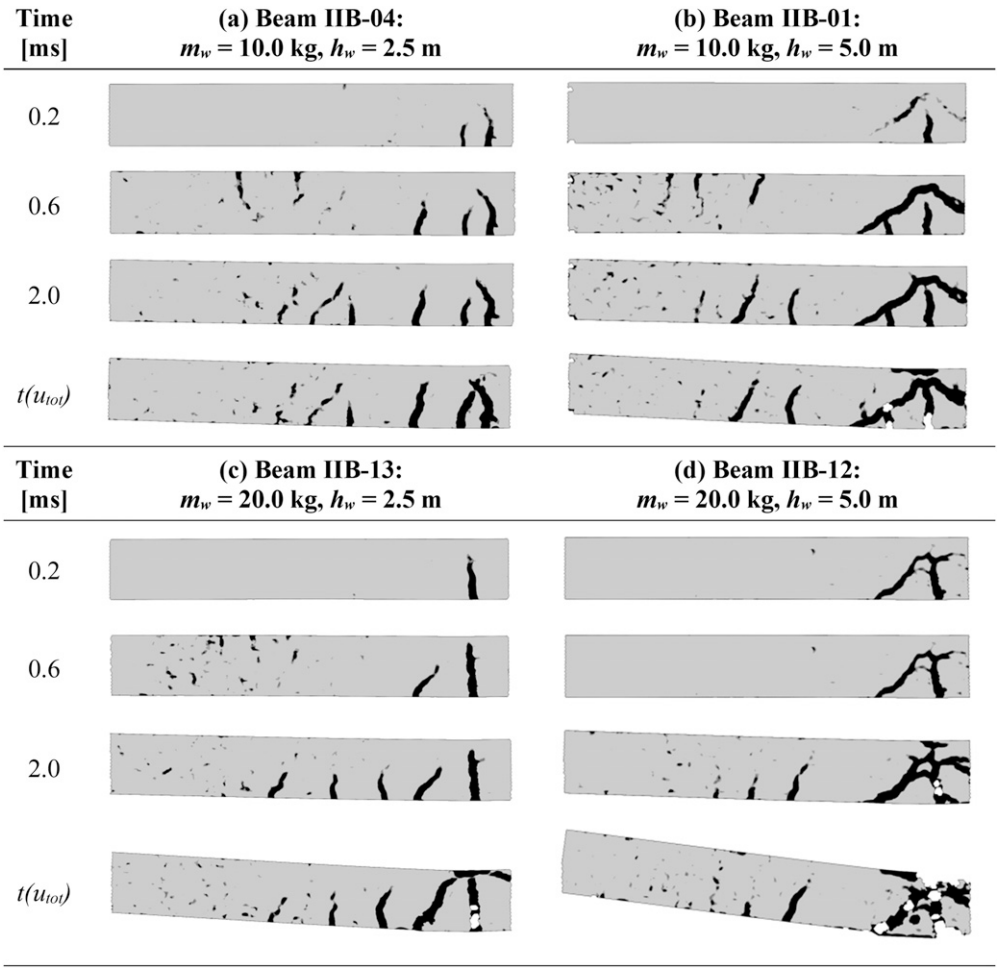

Figure 9. Strain field of first impact for beams in Series II, showing about half the beam. Refer to Figure 3(b) for the FoV.

repeated impacts with the lowest total impact momentum $n{\cdot}I_0$ (beam IIB-01) sustained greater damage than the beam with a larger mass but lower drop height (beam IIB-13). This indicates that with repeated impacts, the impact velocity is more important than the momentum of the drop-weight upon impact.

Results of static tests

Crack formation and load-deflection curves

Figure 11 shows the crack formations from the static tests. In the reference beams, typical flexural and flexural shear cracks developed under loading. In those beams previously subjected to impact loading, the previously created cracks reopened and continued to grow under static loading. In beams subjected to a

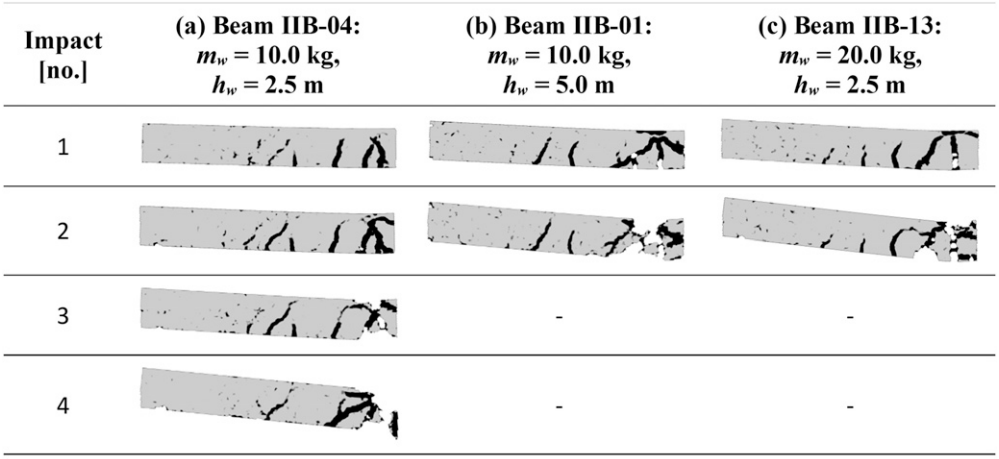

Figure 10. Strain fields for repeated impacts for beams in Series II, showing about half the beam. Refer to Figure 3(b) for the FoV.

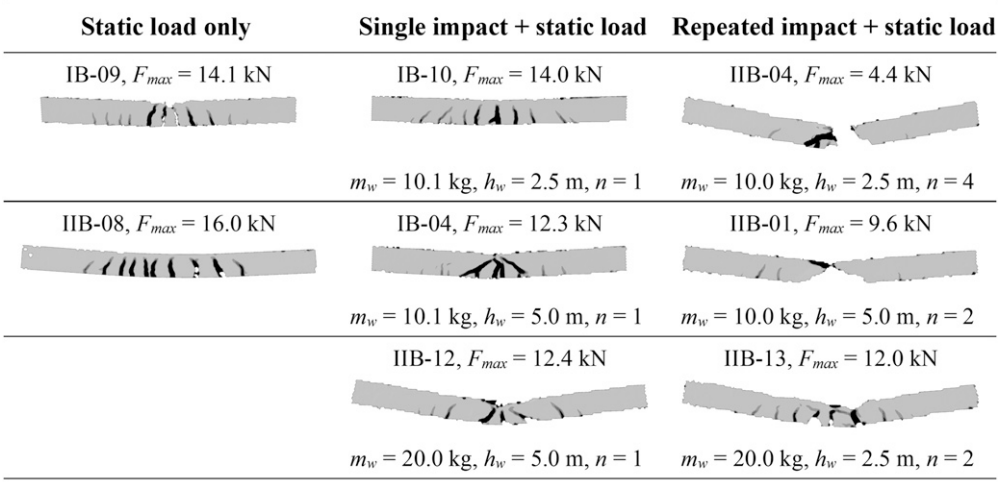

Figure 11. Crack formation from static tests, showing about the whole beam. Refer to Figure 4 for the FoVs.

single impact from a low drop height (beam IB-10), the crack pattern resembled that sustained in the reference beams (although some minor diagonal shear cracks were seen in some of the impact-loaded beams). In contrast, the diagonal shear cracks caused by impact loading were much more pronounced in beams subjected to impact from a greater drop height (beams IB-04 and IIB-12).

In beams subjected to four impacts from a low drop height (beam IIB-04), severe crushing and spalling occurred (the white areas in the figure). Compared to beams IIB-01 and IIB-13, the impact caused more crushing and spalling in beam IIB-01.

Figure 12 shows the load-deflection curves of the statically loaded reference beams. The maximum load F_{max} was in all tests limited by concrete crushing. However, this did not lead to final

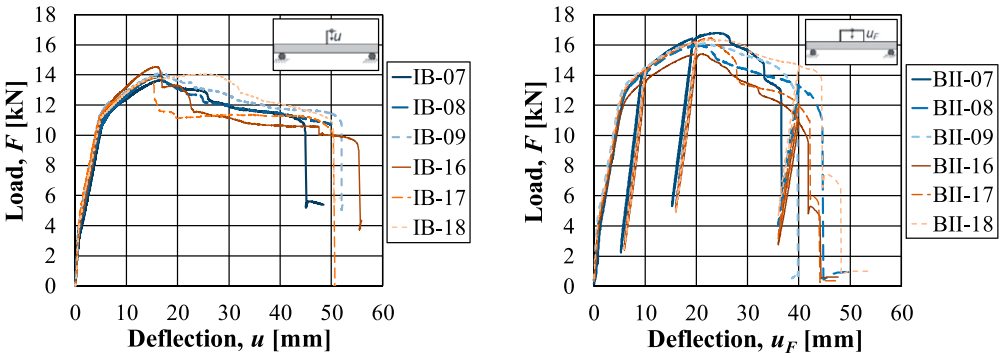

Figure 12. Load-deflection curves of static tests, reference beams.

failure; instead, it resulted in increased deflection accompanied by a reduction in load capacity. Final failure in all tests, except one, was caused by reinforcement rupture, as indicated by the rapid loss of load capacity in Figure 12. Beam IB-08 did not reach failure, as the test was interrupted when the load had decreased by 20% compared to F_{max}. The responses within each test series are fairly similar, and one beam from each series (IB-09 and IIB-08) was chosen to represent the reference beams when comparing with those previously subjected to impact loading, see Figure 13. Here, the plastic deflection after impact is indicated in the graphs as an initial deflection at zero static load.

For single impacts, the initial elastic stiffness of the beams in Series I-1 was very similar to that of the reference beams in the cracked state. However, for the beams in Series I-2 and II-4, the elastic stiffness decreased somewhat compared to those reference beams. Furthermore, when the load-deflection curve $F(u)$ of the beams previously subjected to impact loading reached that of the reference beam, the response subsequently followed approximately the same track up to failure. For Series I-1, both the ultimate load capacity and deflection at failure were in the same order of magnitude as those of the reference beam. However, in Series I-2 and II-4, the ultimate load capacity was somewhat reduced due to damage sustained in the beams from previous impact loading. Additionally, the deflection at final failure increased, leading to higher energy absorption capacity. This indicates that subjecting a beam to high-impact loading may enhance its energy absorption capacity.

Based on the maximum load capacities reached in the tests, bending failure was anticipated in all tests. In most Series I cases, the response was similar to that of the reference beams with the final failure caused by reinforcement rupture. However, in one beam (IB-13) that was initially subjected to impact loading, a distinct shear failure occurred during static loading, resulting in a significant reduction in energy absorption capacity. Using DIC, it was found that this critical shear crack had formed during the previous impact but was manageable up to that point. However, when subjected to subsequent static loading, this critical shear crack opened, causing a shear failure in the beam at a much lower level than in the other tested beams. This shows that a failure mode may be influenced by the loading type and that subsequent static loading may cause failure at lower load levels than those experienced under impact loading. Furthermore, another of the impact-loaded beams in Series I (IB-04) failed due to concrete crushing and was stopped at a low load level under major deflection. In Series II, reinforcement rupture only occurred in five of the beams previously subjected to impact loading (IIB-03, IIB-10, IIB-12, IIB-13, IIB-14). The rest reached final failure due to concrete crushing or were stopped at a low load value under major deflection. Compared to Series I, this behaviour reflects the effect of concrete damage accumulated from repeated impact loading.

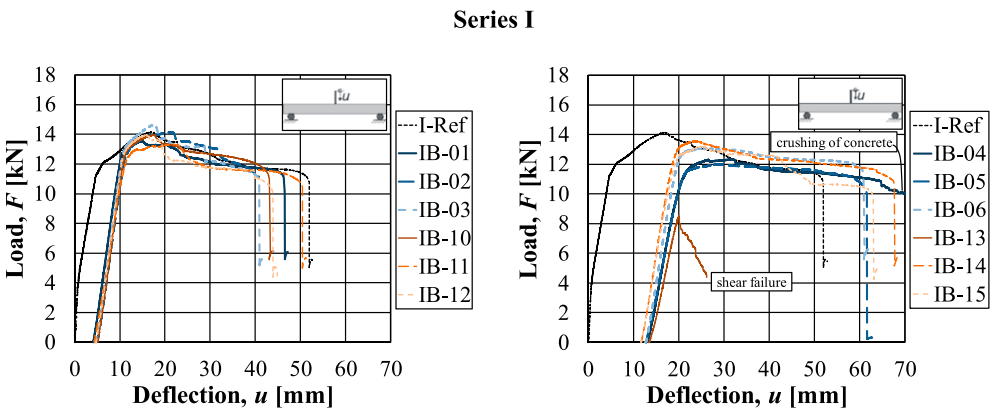

(a) Series I-1: m_w = 10.1 kg, h_w = 2.5 m, n = 1 (b) Series I-2: m_w = 10.1 kg, h_w = 5.0 m, n = 1

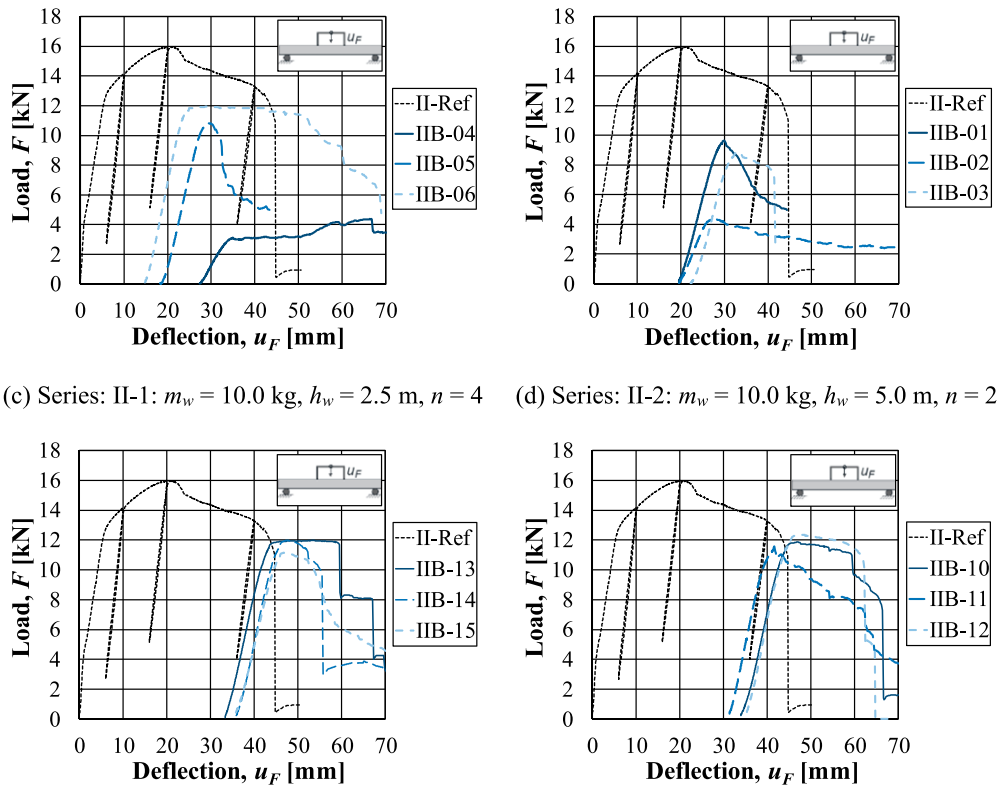

(c) Series: II-1: m_w = 10.0 kg, h_w = 2.5 m, n = 4 (d) Series: II-2: m_w = 10.0 kg, h_w = 5.0 m, n = 2

(e) Series: II-3: m_w = 20.0 kg, h_w = 2.5 m, n = 2 (f) Series: II-4: m_w = 20.0 kg, h_w = 5.0 m, n = 1

Figure 13. Load-deflection curves of static tests. The representative reference beams are IB-09 (Series I) and IIB-08 (Series II).

For repeated impacts, all the beams were subjected to the same total impact energy $n{\cdot}E_{k,0}$ (see Table 3). For the beams in Series II-1 (four impacts) and Series II-2 (two impacts, low mass but high drop height), the scatter was significant and, thus, the residual strength and deflection at failure varied greatly. The beams in Series II-1 sustained the greatest damage, see beam IIB-04 in Figure 10. Due to this, the remaining residual load capacity was very low (F_{max} = 4.4 kN) and the test was stopped once a major deflection had occurred. This indicates that for beams subjected to several repeated impacts, the local damage in the impact zone may become so great that it affects the global residual capacity.

Comparing the beams subjected to two impacts (Series II-2 and II-3), it was noticed that the damage increased with a combination of reduced mass but increased drop height (Series II-2). This indicates that the impact velocity is more important than the momentum of the drop-weight upon impact. For Series II-2, the result was a significantly reduced residual load capacity (F_{max} = 4.3–9.6 kN). However, for Series II-3, the local damage in the beams was less pronounced than in the others that were subjected to repeated impacts. Instead, the response resembled that obtained in the beams of Series I-2 and II-4, which were subjected to one impact only. Due to the previous impact loading, the ultimate load capacity was reduced (F_{max} = 11.1–12.0 kN) but the deflection at failure (due to reinforcement rupture) increased compared to that of the reference beams.

Energy absorption

The total energy absorption capacity $W_{i,tot}$ of the beams was studied. It was defined as:

$$W_{i,tot} = W_{i,sta} + W_{i,imp,pl} \tag{12}$$

in which $W_{i,sta} = W_{i,el} + W_{i,pl}$ is the total energy absorption obtained in static loading and $W_{i,imp,pl}$ is the plastic energy absorption obtained in impact loading. For beams subjected to static loading, the energy absorption was determined as the sum of elastic ($W_{i,el}$) and plastic ($W_{i,pl}$) energy absorption in accordance with equation (10), see Figure 2. In most beams previously subjected to impact loading, the static test was interrupted before reaching total failure (F = 0 kN), meaning that the full energy absorption capacity due to static loading could not be determined. Nevertheless, it was deemed questionable to include the energy absorption contribution from excessively low load values. $W_{i,pl}$ was therefore determined, up to a deflection corresponding to a post-peak load of $F = F_{max}/2$, where F_{max} was determined as the mean maximum load value from the reference beams in each test series.

The method used for static loading cannot be used to estimate the energy absorption under impact loading. A simplified method based on energy equilibrium was used instead, whereby the external energy acting on the beam was determined according to equation (4). Since the same elastic component $W_{i,el}$ is accounted for in both the response to impact loading and subsequent static loading, the contribution from the impact loading was restricted to the plastic energy absorption $W_{i,imp,pl}$.

Using equation (11), the plastic energy absorption due to n number of impacts may be estimated as:

$$W_{i,imp,pl} = \sum_{j=1}^{n} W_{e,j} - n \cdot W_{i,el} \tag{13}$$

in which $W_{e,j}$ is the total external energy applied to the structure (see equation (8)) from impact j and $W_{i,el}$ is the elastic internal energy consumed in the structure in each impact. However, since the

drop-weight mass m_w and external impact velocity v_0 are constant, the external work $W_{e,k}$, resulting from the kinetic energy as defined in equation (4), remains the same for each impact. By combining equations (4) and (8) with equation (13), the plastic energy absorption due to n number of impacts may finally be expressed as:

$$W_{i,imp,pl} = n \cdot \left(\frac{m_w}{m_w + m_b} \cdot E_{k,0} - W_{i,el} \right) + W_{e,p} \tag{14}$$

in which $E_{k,0}$ is determined according to equation (1) and $m_b = \kappa_{LM} \cdot m_{beam}$ is the effective mass of the beam. Assuming a plastic response of the beam (triangular-shaped deflection), the load-mass transformation factor may be expressed as $\kappa_{LM} = 0.333$ (Biggs, 1964). Using $m_{beam} = 25.0$ kg for the 1.0 m long beam part between the supports gives $m_b = 8.3$ kg. The contribution from $W_{e,p}$ caused by a change in potential energy, see equation (7), is very small in these tests (about 5 J and 20 J at most for Series I and II respectively) and is therefore disregarded.

Tables 6 and 7 summarise the results of the impact and static tests in Series I and II, respectively. The energy absorptions according to equations (12) and (14) due to impact and static loading are presented alongside the deflections u and static force F. In Series II, the elastic energy $W_{i,el}$ in equation (14) was based on the mean values measured in Series I (see Table 6) and set to $W_{i,el} = 32$ J.

Table 7 summarises the total energy absorption capacities $W_{i,tot}$ from Tables 6 and 8 and also presents the coefficient of variation (CV) and ratio η_W between $W_{i,tot}$ and $W_{i,tot}$ of the reference beams in that test series. From this, it may be noted that minor scatter (CV = 0.04-0.09) in results was observed in all series except Series II-1. In contrast, the scatter in Series II-1 (four impact loads) was substantial (CV = 0.41).

For Series I (Table 6), the total energy absorption $W_{i,tot}$ for the beams subjected to impact from a drop height $h_w = 2.5$ m was of the same order or slightly lower, averaging a factor of 0.96 compared to the reference beams. However, for the beams subjected to impact from a drop height $h_w = 5.0$ m, the total energy absorption increased, on average, by a factor of 1.42 for the beams that failed in bending.

The increased energy absorption was mainly due to the positive effects of inclined shear cracks caused by the impact (compare beams IB-10 and IB-04 in Figure 11). An increased length of the plastic hinge was thereby obtained. Furthermore, the more intense impact sustained from a higher drop height is believed to have weakened the bond between reinforcement and concrete in this region. Jointly, the presence of shear cracks and reduced bond meant that a longer portion of the reinforcement yielded prior to failure. Since the final failure in all but two beams (IB-04 and IB-13) was caused by ruptured reinforcement, this also resulted in increased deflection and, thus, increased energy absorption. For Series II (Table 8), the total energy absorption for the beams subjected to single impact (Series II-4) increased, on average, by a factor of 1.61 compared to the reference beams.

These results were similar to those obtained in Series I-2, which used the same drop height. However, for repeated impact loading (Series II-1, II-2 and II-3), increased local damage was sustained in the impact zone (see Figure 10) resulting in an ambiguous effect on the total energy absorption capacity. For Series II-1 and II-2, the energy absorption was of the same order, averaging factors of 1.04 and 0.94 respectively, compared to the reference beams. However, the scatter in the results of the residual static tests was substantial, see Figure 13(c) and (d). This was particularly the case in Series II-1, in which two out of three tests resulted in less energy absorption than in any of the reference beams in Series II-ref. However, Series II-3 saw an increase in

Table 6. Summary of results from impact and static tests for Series I. Mean values (standard deviations) are in bold. Standard deviations were only determined where three or more values were available.

Identification		Impact loading			Static loading					Total		
Series	Beam	u_{tot} (mm)	u_0 (mm)	$W_{i,imp,pl}$ (J)	u_0 (mm)	u_{fail} (mm)	F_{max} (kN)	$W_{i,el}$ (J)	$W_{i,pl}$ (J)	$u_{fail,tot}$ (mm)	$W_{i.tot}$ (J)	Type[a]
I-ref	IB-07	—	—	—	—	45.0	13.7	33	486	45.0	519	RR
	IB-08[b]	—	—	—	—	-	13.9	32	346	-	378	NF
	IB-09	—	—	—	—	52.0	14.1	31	594	52.0	625	RR
	IB-16	—	—	—	—	55.4	14.5	33	583	55.4	616	RR
	IB-17	—	—	—	—	50.4	13.8	32	532	50.4	564	RR
	IB-18	—	—	—	—	50.5	14.1	35	582	50.5	617	RR
	mean (std dev)	—	—	—	—	50.7 (3.8)	14.0 (0.3)	33 (1)	555 (46)	50.7 (3.8)	588 (46)	
I-1	IB-01	10.5	4.1	105	4.1	42.4	13.6	31	458	46.5	594	RR
	IB-02	11.0	5.0	106	5.0	36.6	14.1	30	396	41.6	540	RR
	IB-03	10.4	4.7	102	4.7	36.2	14.7	34	393	40.9	529	RR
	IB-10	10.5	5.1	102	5.1	38.0	14.0	34	415	43.1	551	RR
	IB-11	11.2	4.3	106	4.3	46.1	13.3	30	487	50.4	623	RR
	IB-12	10.7	4.7	105	4.7	39.2	14.0	31	411	43.9	547	RR
	mean (std dev)	10.7 (0.3)	4.7 (0.4)	104 (2)	4.7 (0.4)	38.9 (5.0)	14.0 (0.5)	32 (2)	427 (38)	44.4 (3.5)	564 (36)	
I-2	IB-04[c]	20.4	13.0	245	13.0	—	12.3	27	655	—	927	CC
	IB-05	20.6	12.8	239	12.8	48.8	12.0	33	486	61.6	758	RR
	IB-06	20.0	12.7	236	12.7	48.1	13.1	36	523	60.8	795	RR
	IB-13[d]	20.9	13.3	251	13.3	—	8.5	21	21	—	293	SF
	IB-14	19.0	11.7	238	11.7	55.9	13.5	34	614	67.6	886	RR
	IB-15	19.8	11.7	242	11.7	51.4	13.2	30	536	63.1	808	RR
	mean (std dev)	20.1 (0.7)	12.5 (0.7)	242 (5)	12.5 (0.7)	51.1 (3.5)	12.8 (0.6)	32 (4)	563 (70)	63.3 (3.0)	835 (70)	

u_{tot} = total midpoint deflection after impact, u_0 = plastic midpoint deflection after impact.
u_{fail} = deflection under point load at failure in static test, $u_{fail,tot} = u_0 + u_{fail}$.
[a]Type of failure: CC = Concrete crushing, NF = No failure (loading interrupted), RR = Reinforcement rupture, SF = Shear failure.
[b]Static loading interrupted at load level of $0.8 \cdot F_{max}$. This specimen is excluded for mean values of $W_{i,pl}$ and $W_{i,tot}$.
[c]Static loading interrupted at load level of approximately 4 kN at u = 87 mm.
[d]This specimen is excluded for mean values and standard deviation of static loading.

Table 7. Summary of results from impact and static tests for Series II. Mean values (standard deviations) are in bold. Standard deviations were only determined where three or more values were available.

Identification		Impact loading			Static loading					Total		
Series	Beam	$u_{tot,n}$ (mm)	$u_{0,n}$ (mm)	$W_{i,imp,pl}$ (J)	$u_{F,0,n}$ (mm)	$u_{F,fail}$ (mm)	F_{max} (kN)	$W_{i,el}$ (J)	$W_{i,pl}$ (J)	$u_{F,fail,tot}$ (mm)	$W_{i.tot}$ (J)	Type[a]
II-ref	IIB-07	—	—	—	—	36.6	16.8	41	475	36.6	516	RR
	IIB-08	—	—	—	—	44.6	16.0	41	568	44.6	609	RR
	IIB-09	—	—	—	—	39.7	16.1	45	520	39.7	565	RR
	IIB-16	—	—	—	—	41.8	15.4	39	500	41.8	539	RR
	IIB-17	—	—	—	—	42.1	16.5	41	531	42.1	572	RR
	IIB-18	—	—	—	—	44.5	16.3	43	603	44.5	646	RR
	mean (std dev)	—	—	—	—	**41.6 (3.0)**	**16.2 (0.5)**	**42 (2)**	**533 (46)**	**41.6 (3.0)**	**575 (47)**	
II-1	IIB-04[b]	48.9	39.0	408	27.4	—	4.4	9	0	—	417	CC
	IIB-05[b]	35.4	22.3	408	18.3	—	10.8	41	56	—	505	CC
	IIB-06[b]	31.6	19.4	408	14.9	—	11.9	46	420	—	874	CC
	mean (std dev)	**38.6 (9.1)**	**26.9 (10.6)**	**408 (0)**	**20.2 (6.5)**	—	**9.0 (4.1)**	**32 (20)**	**159 (-)**	—	**599 (242)**	
II-2	IIB-01[b]	38.0	31.0	472	19.5	—	9.6	37	52	—	561	CC
	IIB-02[b]	40.3	28.1	472	19.6	—	4.3	12	0	—	484	CC
	IIB-03	40.5	31.2	472	22.2	19.3	8.9	32	63	41.5	567	RR
	mean (std dev)	**39.6 (1.4)**	**30.1 (1.7)**	**472 (0)**	**20.4 (1.5)**	**— (-)**	**7.6 (2.9)**	**27 (13)**	**38 (-)**	**— (-)**	**537 (46)**	
II-3	IIB-13	54.0	40.9	629	33.3	33.8	12.0	44	245	67.1	918	RR
	IIB-14	54.4	44.4	629	35.9	19.6	12.0	46	126	55.5	801	RR
	IIB-15[b]	61.2	49.2	629	35.8	—	11.1	46	118	—	793	CC
	mean (std dev)	**56.5 (4.0)**	**44.8 (4.2)**	**629 (0)**	**35.0 (1.5)**	**26.7 (-)**	**11.7 (0.5)**	**45 (1)**	**163 (71)**	**61.3 (-)**	**837 (70)**	
II-4	IIB-10	59.8	46.1	661	34.0	31.6	11.9	47	246	65.6	954	RR
	IIB-11[b]	54.8	41.9	661	31.4	—	11.6	44	184	—	889	CC
	IIB-12	57.7	45.8	661	35.3	27.1	12.4	40	231	62.4	932	RR
	mean (std dev)	**57.4 (2.5)**	**44.6 (2.3)**	**661 (0)**	**33.6 (2.0)**	**29.4 (-)**	**12.0 (0.4)**	**44 (4)**	**220 (32)**	**64.0 (-)**	**925 (33)**	

$u_{tot,n}$ = total midpoint deflection after n impacts, $u_{0,n}$ = total plastic midpoint deflection after n impacts, $u_{F,0,n}$ = total plastic deflection under point load after n impacts, $u_{F,fail}$ = deflection under point load at failure in static test, $u_{F,fail,tot} = u_{F,0,n} + u_{F,fail}$.

[a]Type of failure: CC = Concrete crushing, RR = Reinforcement rupture.

[b]Static loading interrupted at a load level of 2–5 kN.

Table 8. Comparison of energy absorption capacity.

Series	m_w (kg)	h_w (m)	n [no.]	$W_{i,tot}$ Mean (J)	$W_{i,tot}$ CV [-][a]	η_W [-][b]
I-ref	—	—	—	588	0.08	1.00
I-1	10.1	2.5	1	564	0.06	0.96
I-2	10.1	5.0	1	835	0.08	1.42
II-ref	—	—	—	575	0.08	1.00
II-1	10.0	2.5	4	599	0.41	1.04
II-2	10.0	5.0	2	537	0.09	0.94
II-3	20.0	2.5	2	837	0.08	1.46
II-4	20.0	5.0	1	925	0.04	1.61

[a]Coefficient of variation: CV = std dev/mean.
[b]Ratio of energy absorption capacity: $\eta_W = W_{i,tot}/W_{i,tot,ref}$.

absorption energy (averaging a factor of 1.46), despite these beams also being subjected to repeated impact loading.

When comparing Series II-2 and II-3 (different drop-weight mass and drop height), Table 3 shows that the number of impacts ($n = 2$) and accumulated impact energy ($n{\cdot}E_{k,0} = 981$ J) were the same. Furthermore, the accumulated impact impulse and permanent deflection were greater for the beams in Series II-3; $n{\cdot}I_0 = 198$ Ns and $u_{0,2} \approx 30$ mm in Series II-2 compared to 280 Ns and 45 mm in Series II-3. Despite this, the beams in Series II-3 showed a much higher (on average, by a factor of 1.56) energy absorption capacity than those in Series II-2. The crucial difference here seems to have been that the impact velocity was greater in Series II-2 ($v_0 = 9.9$ m/s) than in Series II-3 ($v_0 = 7.0$ m/s). Comparing Series II-1 and II-3 (different drop-weight mass and number of impacts), further reveals the negative influence of repeated loading. Here, the accumulated impact energy ($n{\cdot}E_{k,0} = 981$ J) and impact impulse ($n{\cdot}I_0 = 280$ Ns) were the same. Nevertheless, the energy absorption capacity was noticeably higher (on average, by a factor of 1.40) for the beams in Series II-3.

Conclusions

Two test series of drop-weight impact tests for small-scale RC beams were performed, using a high-speed camera and digital image correlation (DIC) to study deflections and concrete crack patterns. The beams were first subjected to single or repeated impacts using a drop-weight of 10 or 20 kg released from a height of 2.5 or 5.0 m. They were then loaded statically until failure. The results from this were compared with reference beams that were only subjected to static loading. The focus of the study was to investigate the effect of single and repeated impact loading on the structure's total energy absorption capacity.

The following conclusions may be drawn:

- In beams initially subjected to a single impact, the energy absorption capacity was of the same or higher order as in beams subjected solely to static loading. A strong impact resulted in a greater increase of energy absorption than a weak impact; at a drop height of 5.0 m, the increase was about 40% and 60% for drop-weights of 10 kg and 20 kg respectively. Overall, the scatter in total energy absorption capacity was small ($CV \leq 0.08$) for all tests subjected to a single impact load.

- For repeated impacts, the damage sustained in the beam for each successive impact was more severe than that in the previous one. This suggests that repeated, lower-magnitude impacts cause more damage than a single impact of equivalent total impact energy. Additionally, these results indicate that repeated impact loading, especially at high impact velocities, may significantly reduce the structure's energy absorption capacity.
- The residual load capacity of the statically loaded structure decreased as the number of impacts increased. For cases with impact energy and the same number of impacts, greater damage was observed when the drop-weight had a higher velocity. This is despite the higher impact impulse obtained from a drop-weight of higher mass but lower impact velocity. Repeated impacts at lower velocity resulted in approximately 50% higher energy absorption capacity. This suggests that impact velocity is more important than the magnitude of the impact impulse in determining structural damage and energy absorption capacity.
- The final crack formation was determined by the first impact and depended on the magnitude of the impact loading. It could, therefore, differ considerably compared to that obtained solely from static loading. When the drop-weight was released from a height of 2.5 m, the result was bending cracks resembling those sustained in static loading. However, in tests in which the drop-weight was released from a height of 5.0 m, large diagonal shear cracks appeared next to the impact zone.
- The failure mode may change due to impact loading. Bending failure was anticipated in all beams tested. However, one of the beams that was subjected to a single impact exhibited a shear failure at a much lower load level, when subsequently subjected to static loading. This indicates a possible risk of reduced residual static load capacity for impact-loaded structures.
- Overall, beams subjected to one to three impacts demonstrated good repeatability, with a small coefficient of variation (CV) for the maximum deflection: ≤ 0.03 for beams subjected to one impact and ≤ 0.09 for those subjected to two or three. Good repeatability was also obtained for the maximum force in statically loaded beams previously subjected to no ($CV \leq 0.03$) or one ($CV \leq 0.05$) impact. However, for beams subjected to two to four impacts, the static residual response showed considerable scatter.
- The study presented here was performed on small-scale beams. However, size effects influence the results and increased beam depth leads to increased brittleness and thus decreased energy absorption capacity. A follow-up study, in which beams with larger depths and various reinforcement amounts are used, would therefore be valuable.
- High-speed DIC analyses may be effective in studying the dynamic response of beams subjected to impact loading, whilst allowing deflections and crack propagation to be monitored in detail.

Acknowledgements

This research has been carried out in collaboration with Chalmers University of Technology and RISE Research Institutes of Sweden. The authors would like to thank the financier's representative Lars Gråbergs (BSc), from the Swedish Civil Contingencies Agency (MSB). Thanks also to research engineer Sebastian Almfeldt (MSc), Chalmers, for his expertise and guidance with the experiments. Additionally, Leo Laine (PhD), LL Engineering, is highly acknowledged for his support.

Declaration of conflicting interests

The authors declared no potential conflicts of interest with respect to the research, authorship, and/or publication of this article.

Funding

The authors disclosed receipt of the following financial support for the research, authorship, and/or publication of this article: This work was supported by the Swedish Civil Contingencies Agency (MSB). Additional funding for the experiments was provided by Fortifikationskårens forskningsfond (Fortification corps' research fund).

Ethical statement

Informed consent

The research was conducted to the highest possible ethical standards, and all authors consent to publication.

ORCID iDs

Morgan Johansson https://orcid.org/0000-0003-0020-0646
Joosef Leppänen https://orcid.org/0000-0001-8620-8790
Fabio Lozano https://orcid.org/0000-0002-3935-4223

Data Availability Statement

Research data will be shared in public data repository according to section data availability. The data that support the findings of this study are openly available in the dataset at https://doi.org/10.5281/zenodo.12578464 (Leppänen, 2025).

References

Adhikary SD, Li B and Fujikake K (2012) Dynamic behavior of reinforced concrete beams under varying rates of concentrated loading. *International Journal of Impact Engineering* 47: 24–38.

Adhikary SD, Li B and Fujikake K (2015) Residual resistance of impact-damaged reinforced concrete beams. *Magazine of Concrete Research* 67(7): 364–378.

Aramis (2018) Aramis 12 M. https://www.zeiss.com/metrology/en/explore/topics/aramis-high-speed-dic-systems.html

Barr B and Bouamrata A (1988) Development of a repeated dropweight impact testing apparatus for studying fibre reinforced concrete materials. *Composites* 19(6): 453–466.

Batarlar B, Hering M, Bracklow F, et al. (2021) Experimental investigation on reinforced concrete slabs strengthened with carbon textiles under repeated impact loads. *Structural Concrete* 22(1): 120–131.

Bigaj AJ (1999) *Structural Dependence of Rotational Capacity of Plastic Hinges in RC Beams and Slabs* [PhD Dissertation]. Delft, The Netherlands: TU Delft, Civil Engineering and Geosciences.

Biggs JM (1964) *Introduction to Structural Dynamics*. New-York, USA: McGraw-Hill.

Bischoff PH and Perry SH (1991) Compressive behaviour of concrete at high strain rates. *Materials and Structures* 24(6): 425–450.

Carpinteri A, Corrado M, Mancini G, et al. (2009) Size-scale effects on plastic rotational capacity of reinforced concrete beams. *ACI Structural Journal* 106(6). DOI: 10.14359/51663190.

CEN 2004. (2009) *EN 12390-3: testing hardened concrete - Part 3: compressive strength of test specimens* (Issue 138227).

Cui L, Zhang X and Hao H (2023) Improved analysis for impact response prediction of reinforced concrete structures considering stress wave propagation and time dependent shape function. *International Journal of Impact Engineering* 182: 104783.

DOD (2008) *Structures to Resist the Effects of Accidental Explosions (UFC 3-340-02)*. USA: Department of Defence.

Fujikake K, Senga T, Ueda N, et al. (2006) Study on impact response of reactive powder concrete beam and its analytical model. *Journal of Advanced Concrete Technology* 4(1): 99–108.

Fujikake K, Li B and Soeun S (2009) Impact response of reinforced concrete beam and its analytical evaluation. *Journal of Structural Engineering* 135(8): 938–950.

GOM (2018) GOM correlate professional, Hotfix 5. https://www.zeiss.com/metrology/en/software/metrology-software.html

Isaac P, Darby A, Ibell T, et al. (2017) Experimental investigation into the force propagation velocity due to hard impacts on reinforced concrete members. *International Journal of Impact Engineering* 100: 131–138.

Johansson M and Laine L (2012) *Bebyggelsens motståndsförmåga mot extrem dynamisk belastning Del 3: Kapacitet hos byggnader (MSB142). (The resistance of housing settlement subjected to extreme dynamic loading. Part 3: building capacity. In Swedish). Swedish Civil Contingencies Agency, S.*

Johansson M, Rempling R, De Ulzurrun GSD, et al. (2019) Key aspects of digital image correlation in impact tests of reinforced concrete beams. *IABSE Reports* 114: 961–968.

Johansson M, Leppänen J, Andersson M, et al. (2024) Residual capacity of RC beams subjected to impact loading: influence of reinforcement ductility. *International Journal of Protective Structures*. DOI: 10.1177/20414196241277221.

Jönsson J and Stenseke A (2018) *Concrete Beams Subjected to Repeated Drop-Weight Impact and Static Load, Assessment of Structural Response in Experimental Testing and Predicted Response with Numerical Analyses*. [Master's Thesis ACEX30-18-34]. Master's Thesis ACEX30-18-34. Chalmers University of Technology, Department of Architecture and Civil Engineering.

Kang THK, Nghiem A, Demartino C, et al. (2025) Structural resilience of post-tensioned members to repeated low-velocity impacts. *Engineering Structures* 330: 119902.

Kishi N, Mikami H, Matsuoka KG, et al. (2002) Impact behavior of shear-failure-type RC beams without shear rebar. *International Journal of Impact Engineering* 27(9): 955–968.

Leppänen J (2025) Dataset of article: experimental analysis of total energy absorption capacity in RC beams subjected to single or repeated drop-weight impacts. DOI: 10.5281/zenodo.12578464.

Leppänen J, Johansson M and Grassl P (2020) On the dynamic response of reinforced concrete beams subjected to drop weight impact. *Finite Elements in Analysis and Design* 180: 103438.

Li G, Tan KH and Fung TC (2020) Experimental study on CFRP-concrete dynamic debonding behaviour. *Engineering Structures* 206: 110055.

Löfgren I, Olesen JF and Flansbjer M (2004) *Application of WST-Method for Fracture Testing of Fibre-Reinforced Concrete, Chalmers University of Technology, Department of Structural Engineering and Mechanics, Report 04:13*. Issue 0170.

Lovén J and Svavarsdóttir ES (2016) *Concrete Beams Subjected to Drop Weight Impact: Comparison of Experimental Data and Numerical Modelling*. Master's Thesis. Chalmers University of Technology.

Lozano F and Makdesi J (2017) *Concrete Beams Subjected to Drop-Weight Impact and Static Load, Structural Behavior and Plastic Rotational Capacity from Experiments and Finite Element Analysis*. [Master's Thesis BOMX02-17-21]. Master's Thesis BOMX02-17-21. Chalmers University of Technology, Department of Architecture and Civil Engineering.

Magnusson J and Hallgren H (2003) *High Performance Concrete Beams Subjected to Shock Waves from Air Blast, Part 2. (Report R–1116–SE), Swedish Defence Research Establishment (FOA), Sweden*.

Magnusson J, Hallgren M and Ansell A (2014) Shear in concrete structures subjected to dynamic loads. *Structural Concrete* 15(1): 55–65.

Malvar LJ (1998) Review of static and dynamic properties of steel reinforcing bars. *ACI Materials Journal* 95(5): 609–616.

Malvar LJ and Ross CA (1998) Review of strain rate effects for concrete in tension. *ACI Materials Journal* 95(6): 735–739.

Mier J, Pruijssers A, Reinhardt H, et al. (1991) Load-time response of colliding concrete bodies. *Journal of Structural Engineering-ASCE* 117(2): 354–374.

Othman H and Marzouk H (2016) An experimental investigation on the effect of steel reinforcement on impact response of reinforced concrete plates. *International Journal of Impact Engineering* 88: 12–21.

Pham TM, Hao Y and Hao H (2018) Sensitivity of impact behaviour of RC beams to contact stiffness. *International Journal of Impact Engineering* 112: 155–164.

Pritchard RH, Lava P, Debruyne D, et al. (2013) Precise determination of the Poisson ratio in soft materials with 2D digital image correlation. *Soft Matter* 9(26): 6037–6045.

Reu P (2012) Introduction to digital image correlation: best practices and applications. *Experimental Techniques* 36(1): 3–4.

Reu PL and Miller TJ (2008) The application of high-speed digital image correlation. *The Journal of Strain Analysis for Engineering Design* 43(8): 673–688.

Saatci S and Vecchio FJ (2009) Effects of shear mechanisms on impact behavior of reinforced concrete beams. *ACI Structural Journal* 106(1): 78–86.

Said AMI and Mabrook Mouwainea E (2022) Experimental investigation on reinforced concrete slabs under high-mass low velocity repeated impact loads. *Structures* 35: 314–324.

Sharma R and Kasilingam S (2024) Performance of thin reinforced concrete slabs against low velocity repeated impact load. *European Journal of Environmental and Civil Engineering* 28(6): 1415–1444.

Sutton MA, Orteu JJ and Schreier H (2009) *Image correlation for shape, motion and deformation measurements: Basic concepts, theory and applications*. Berlin: Springer. DOI: 10.1007/978-0-387-78747-3.

Swedish Fortifications Agency (2011) *Building Regulations FKR 2011. Dnr. 4535/2011 (In Swedish). Eskilstuna, Sweden*.

Ulzurrun GSD and Zanuy C (2024) Dynamic shear force-bending moment interaction diagrams in RC beams under impact. *Engineering Structures* 308(2024): 118021.

Ulzurrun GSD, Zanuy C, Johansson M, et al. (2019) Impact propagation effects along reinforced concrete beams.

Yi W-J, Zhao D-B and Kunnath SK (2016) Simplified approach for assessing shear resistance of reinforced concrete beams under impact loads. *ACI Structural Journal* 113(4): 747–756.

Yilmaz C, Kirtel O, Dok G, et al. (2023) Experimental investigation on the post-impact behavior of normal-strength reinforced concrete beams subjected to drop-weight impact loads. *Arabian Journal for Science and Engineering* 48(10): 13241–13258.

Zhang XX, Ruiz G and Yu RC (2010) A new drop-weight impact machine for studying fracture processes in structural concrete. *Strain* 46(3): 252–257.

Zhang J, Wang R, Zhang Z, et al. (2023) Residual performance and damage mechanism of prestressed concrete box girder bridge subjected to falling heavy object impact. *Structure and Infrastructure Engineering* 19(11): 1568–1584.